A low-cost photoactive composite quartz sand/TiO_2

Jonáš Tokarský[a,*], Vlastimil Matějka[a], Lucie Neuwirthová[a], Jiřina Vontorová[b], Kateřina Mamulová Kutláková[a], Jana Kukutschová[a], Pavla Čapková[c]

[a] Nanotechnology Centre, VŠB-Technical University of Ostrava, 17. listopadu 15/2172, 708 33 Ostrava-Poruba, Czech Republic.

[b] Department of analytical chemistry and material testing, Faculty of Metallurgy and Materials Testing, VŠB-Technical University of Ostrava, 17. listopadu 15/2172, 708 33 Ostrava-Poruba, Czech Republic.

[c] Faculty of Science, J. E. Purkyně University, České mládeže 8,400 96 Ústi nad Labem, Czech Republic

Abstract

The photoactive quartz sand/TiO_2 composites were prepared by thermal hydrolysis of the suspension obtained by addition of quartz sand to a titanyl sulfate solution. The required amount of TiO_2 in the prepared composites (i.e 9, 22 and 45 wt. %, respectively) was achieved using a variable titanyl sulfate/quartz ratio. As reference materials, pure TiO_2 was prepared using the thermal hydrolysis of the titanyl sulfate solution under the same condition as used during the preparation of composite quartz/TiO_2. The composite samples, dried at 105°C and calcined at temperatures of 500–900°C, were investigated using X-ray fluorescence spectroscopy, X-ray powder diffraction analysis, transmission electron microscopy, and Fourier transform infrared spectroscopy. Structural ordering of TiO_2 particles on the quartz surface was studied using atomistic simulations in a Material Studio modeling environment. Photodegradation activity of the composites was evaluated by the discoloration of Acid Orange 7 aqueous solution. The composite containing 22 wt.% of TiO_2 and calcined at 800°C exhibits the highest photoactivity. Higher and lower amounts of TiO_2 led to worse results. The quartz/TiO_2 composite is a promising material able to replace pure TiO_2 in a wide range of building materials.

Keywords: quartz sand; TiO_2; nanocomposite; photoactivity

*Corresponding author

E-mail address: jonas.tokarsky@vsb.cz (J. Tokarský)

Tel.: +420 597 321 519; Fax: +420 597 321 640

Abbreviations: E_{ad} – *adhesion energy [kcal]*, E_{tot} – *total energy of the nanocomposite [kcal]*, $E_{tot,SiO2}$ – *total energy of the SiO_2 substrate [kcal]*, $E_{tot,TiO2}$ – *total energy of the TiO_2 nanoparticle [kcal]*, MS – *Accelrys Materials Studio modeling environment*, QEq – *charge equilibration method*, $SiO_2(1)$ – *pure SiO_2 powder dried at 105 °C*, $SiO_2(6)$ – *pure SiO_2 powder calcined at 600 °C*, SITI – *titanium oxide nanoparticles/SiO_2 nanocomposite,* SITI11 – *composite dried at 105 °C and containing 10 wt.% of TiO_2*, SITI12 – *composite dried at 105 °C and containing 20 wt.% of TiO_2*, SITI15 – *composite dried at 105 °C and containing 50 wt.% of TiO_2*, SITI61 – *composite calcined at 600 °C and containing 10 wt.% of TiO_2*, SITI62 – *composite calcined at 600 °C and containing 20 wt.% of TiO_2*, SITI65 – *composite calcined at 600 °C and containing 50 wt.% of TiO_2*, $TiO_2(1)$ – *pure TiO_2 powder dried at 105 °C*, $TiO_2(6)$ – *pure TiO_2 powder calcined at 600 °C*, UFF – *Universal Force Field*

1. Introduction

Titanium dioxide (TiO_2) in its nano-form is today the most frequently studied photocatalyst. The surface and structural properties of TiO_2 are summarized in detail by Diebold [1]. The TiO_2 group is composed of three modifications - anatase, brookite and rutile. Among them, the anatase is a modification with promising properties due to its high photocatalytic activity. The principle of the photodegradation mechanism of TiO_2 can be found in the article published by Fujishima and his co-workers [2].

TiO_2 nanoparticles can be prepared using a wide scale of synthesis methods [3]. The sol–gel process is the most frequently used, and the common precursors are titanium (IV) alkoxides, mainly titanium (IV) tetraisopropoxide, and titanium (IV) n-butoxide (or titanium (IV) tert-butoxide) [4,5]. The main disadvantage of these precursors is that they are too expensive to be employed for the preparation of TiO_2 nanoparticles in large amounts. Therefore, a large effort has been devoted towards the use of low cost intermediates: mainly titanium tetrachloride ($TiCl_4$) [6,7] and titanylsulfate ($TiOSO_4$) [8,9], which are obtained during the chloride or the sulfate procedure of the TiO_2 white-pigment manufacturing.

The main application of the anatase form of TiO_2 is in the field of photocatalysis, especially degradation of environmental contaminants. This is proven by degradation of model substances presented in liquid and/or in gaseous phase. The TiO_2 can be used for the degradation of pesticides [10], phenol [11,12] and organic dyes [13,14,15] in contaminated waters (i.e. in liquid phase). In a gaseous phase the degradation of formaldehyde [16], toluene [17,18] and nitric oxides [6,19] has been studied.

The photodegradation test with organic dyes represents a fast and easy estimation of TiO_2 photodegradation activity. The rate of the degradation can be monitored by the change in the absorption of the dye solution by the UV-VIS spectrometry. In the case when TiO_2 forms a finely dispersed suspension in a dye solution, the photocatalyst has to be removed by filtration or ultracentrifugation before a measurement of UV-VIS absorption. The complete separation of TiO_2 is almost impossible if its size is in the order of nanometers. If the TiO_2 nanoparticles are fixed on the surface of a suitable particulate substrate, then the separation of the photocatalyst can be easily made by filtration or, for bigger substrate particles, by sedimentation.

Previously a large amount of work has been done in the field of toxicity of TiO_2 nanoparticles against water organisms. It was found that nanoparticles do not necessarily have to enter the cells to cause the toxicity, and that nanoparticles could cause toxic effects despite that they

formed aggregates in suspensions [20,21]. Zhu and his co-workers found that TiO_2 nanoparticles exerted minimal toxicity to freshwater crustacean *Daphnia magna* within the traditional 48 h exposure time, but caused high toxicity when the exposure time was extended to 72 h. Therefore, it seems that TiO_2 nanoparticles exposure, especially for long periods of time, may exert a negative impact on a population of aquatic organisms and on food web dynamics in aquatic systems [22].

An excellent method to avoid (or at least minimize) these risks is a growing and anchoring of the TiO_2 nanoparticles on the surface of a suitable substrate, which prevents the release of TiO_2 nanoparticles to the environment. Moreover, nanocomposites containing nanoparticles directly anchored on the carrier exhibit improved functional properties over simple mechanical mixtures [23,24]

Many substrates have already been studied for anchoring of the TiO_2 on their surface. Preparation of a TiO_2 thin layer on glass substrates by dip or spin coating is widely investigated [25,26]. The resulting glass exhibits anti-fogging and self-cleaning properties. Silica particles are also studied as a matrix for TiO_2 growth and many authors showed that the prepared silica/TiO_2 composites have improved photodegradation activity against model pollutants, such as methyl orange [14], methyl blue [27], 4-nitrophenol [6] and toluene [18].

SiO_2 is very often the natural part of building materials and, therefore, represents an ideal matrix for TiO_2 nanoparticles. Replacing the pure TiO_2 nanoparticles by the photoactive SiO_2/TiO_2 composite can help to reduce all environmental hazards and risks. But the above mentioned approach (i.e. synthesis of SiO_2), however, causes an increase of the final cost and complicates the mass production. Therefore, in the present study we made an attempt to reduce the cost of these photoactive composites by using the quartz sand instead of pure silica. We believe that these composites are useful for dealing with environmental pollution and the necessary condition for their extensive use in building industry is optimum price-efficiency ratio.

This work is focused on the preparation and characterization of the quartz sand/TiO_2 composites using thermal hydrolysis of quartz sand and $TiOSO_4$ suspension. The composites containing 9, 22 and 45 wt.% of TiO_2 were prepared using a simple hydrothermal procedure. Photoactivity of the prepared composites was evaluated by means of photodegradation of Acid Orange 7 (AO7) model solution. Moreover, atomistic simulations using an empirical force field in the Materials Studio (*MS*) modeling environment was carried out in order to study structure and adhesion forces in the quartz/TiO_2 composite.

2. Materials and methods

2.1. Sample preparation

The quartz sand / TiO_2 composites were prepared by thermal hydrolysis of the suspension of quartz sand in the $TiOSO_4$ solution (Precheza a.s.). The quartz sand was used as received, without any further treatment. $TiOSO_4$ contains 90 g of TiO_2 per 1 dm^3 of its suspension in concentrated H_2SO_4. The required amount of TiO_2 in final composite can be achieved by the setting of the appropriate quartz sand/$TiOSO_4$ ratio. The first step of composites preparation includes 1h mixing of the suspension of quartz in $TiOSO_4$ at room temperature. In the second step, the suspension is heated up to 100 °C. The third step includes 90 min long thermal hydrolysis of the suspension at 100 °C performed by addition of the appropriate volume of water (having the temperature 100°C) in the volume ratio of 1:1 with respect to the volume of $TiOSO_4$. After the thermal hydrolysis the reaction mixture is cooled down, then the supernatant liquor is separated by filtration, and the solid portion is washed several times using distilled water to achieve the conductivity of the filtrate of less than 1 $mS \cdot cm^{-1}$. Finally, the resulting sample is dried in an oven at 105 °C. The resulting composite samples are denoted as SITI-*1*-*X*. In this assignment the number *1* means that the samples were dried at 105 °C, letter *X* represents TiO_2 content where *9*, *22* and *45* means 9, 22 and 45 wt.%. of TiO_2, respectively. Further, approximately 1 g of each of the prepared composite is calcined for 1h at selected temperatures and the samples denoted as SITI-*T*-*X* are obtained. At this assignment the letter *T* denotes the temperature of calcination (i.e. numbers *5*, *6*, *7*, *8* and *9* are used for 500, 600, 700, 800 and 900 °C, respectively). Letter *X* has the same meaning as for the dried composites SITI-*1*-*X*. The samples of pure TiO_2 were assigned as TiO_2-*T*, where the letter *T* again denotes the temperature of heat treatment. Pure quartz sand is denoted as SiO_2-*T* in tables or figures and the letter *T* has the same meaning as for the TiO_2-*T*.

2.2. Characterization methods

Chemical composition of prepared samples was determined by X-ray fluorescence spectroscopy (XRFS) using SPECTRO XEPOS (SPECTRO Analytical Instruments GmbH, Germany) equipped with 50 W Pd X-ray tube. Samples were prepared in the form of pressed pellets. Wax was used as a binder.

The X-ray powder diffraction (XRPD) patterns of powder samples were recorded under CoKα irradiation (λ = 1.789 nm) using Bruker D8 Advance diffractometer (Bruker AXS, Germany)

equipped with fast position sensitive detector VÅNTEC 1. Powder samples were pressed in a rotational holder and measurements were carried out in the reflection mode. Lanthanum hexaboride (LaB_6) was used as a standard. Phase composition was evaluated using the PDF 2 Release 2004 database (International Centre for Diffraction Data).

The morphology of the composite particles in the powder samples was observed on transmission electron microscope (TEM) JEOL 2010F (JEOL Ltd., Japan). LaB_6 crystal was used as an electron source.

Mid-infrared (IR) spectra were obtained by Fourier transform infrared spectrometer Nicolet 6700 (Thermo Fisher Scientific, USA) using the single reflection ATR technique on a diamond crystal. Measurements were performed with a resolution of 4 cm^{-1} and 32 scans. Achieved data were processed using the OMNIC software.

The content of sulfur in the powder samples was determined using LECO CS244 equipped with an induction furnace HT1000 (LECO Corporation, USA). The combustion process was realized in ceramic crucibles filled with 1g of flux LECOCEL (tungsten particulates) and 1g of iron chip accelerator.

Specific surface area (SSA) was determined at liquid-nitrogen temperature using Sorptomatic 1990 (Thermo Fisher Scientific, USA), employing the BET methodology. Nitrogen gas was used as the adsorbate.

The method for testing of the photodegradation activity of the prepared composites is based on the degradation of model organic compound, Acid Orange 7 (AO7), after irradiation with UV light. In the first step two identical suspensions containing 50 mg of the composite, 65 ml of deionized water and 5 ml of the AO7 aqueous solution ($c = 6.259 \cdot 10^{-4}$ $mol \cdot dm^{-3}$) were stirred in the dark for 60 min to achieve the absorption equilibrium. After this period one suspension was filtered and the obtained filtrate was stored in the dark. Concentration of AO7 in this filtrate is denoted as c_0. The second suspension was subjected to 60 and 300 min long irradiation using a Pen Ray lamp (intensity of the irradiation measured at 365 nm is 2 $mW \cdot cm^{-3}$) and subsequently filtered. Concentrations of AO7 in these suspensions are denoted as c_t where t means the length of irradiation in minutes. The values of absorbance of filtrates at 450 nm from which the concentrations were calculated are measured using a CINTRA 303 UV-VIS spectrometer. Relative loss of AO7 (i.e. the photoactivity of the sample) is quantified using the following formula

$$photoactivity = \left(1 - \frac{c_t}{c_0}\right) \cdot 100 \qquad (1).$$

Both the geometry optimization and the energy calculation were carried out in *Accelrys Materials Studio* (*MS*) modeling environment/Forcite module. A smart algorithm was used for the geometry optimization with 50,000 iterations. Universal force field (UFF) was used for the energy calculation and the atom based summation method was used to calculate the Coulombic and the van der Waals energy.

3. Results and discussion

3.1. Chemical and phase composition of the samples

The chemical composition of quartz sand and the resulting composites SITI-*1-9*, SITI-*1-22* and SITI-*1-45* can be seen in Table 1.

Table 1
Chemical composition of quartz sand and the prepared composites SITI-*1-9*, SITI-*1-22* and SITI-*1-45* (in wt.%). LOD, loss on drying; LOI, loss on ignition (1000 °C).

	quartz sand	SITI-1-9	SITI-1-22	SITI-1-45
Al_2O_3	1.6	1.4	1.2	0.835
CaO	0.027	0.052	0.098	0.195
K_2O	0.026	0.205	0.172	0.124
MgO	0.020	0.018	0.009	0.008
Na_2O	<0.020	0.140	0.116	0.085
SO_3	0.170	1.5	4.1	8.1
SiO_2	96.9	86.7	73.0	47.6
TiO_2	0.062	8.0	18.6	39.0
LOD	0.041	0.890	2.3	4.5
LOI	0.2	2.5	6.0	12.1

The measured real content (8.0, 18.6 and 39 wt.%) of TiO_2 is lower than the expected TiO_2 content (9, 22 and 45 wt.%) showing the yield approx. 87 % with respect to the theoretical content of TiO_2. It is evident that the amount of the sulfur (remaining in the samples as a remnant of the $TiOSO_4$ precursor) as well as LOD and LOI increases with the increase of the TiO_2 content. The increasing content of the sulfur in the composites is probably connected to the presence of free sulfuric acid, which in fact represents a dispersion medium for TiO_2 in $TiOSO_4$ colloid suspension. With the sulfur content growing, the amount of absorbed water (expressed by LOD) also increases. Sulfuric acid is a strongly hygroscopic compound and is responsible for the presence of the physically absorbed water, which is easily removed at relatively low temperatures. The values of LOI also increase with the TiO_2 content, and these

values comprise the presence of sulfur (in a form of sulfuric acid), and chemically bonded water in $TiO_2 \cdot nH_2O$, which is the main product of the $TiOSO_4$ thermal hydrolysis.

The dependency of the sulfur content on the amount of TiO_2 and calcinations temperature is shown in Table 2, whereas it is evident that the last most significant decrease in the sulfur content was observed at 800 ºC.

Table 2
The dependence of sulfur content [wt.%] on the amount of TiO_2 in SITI composites and calcinations temperature.

TiO_2 content in SITI [wt.%]	temperature [°C]					
	105	500	600	700	800	900
9	0.599	0.311	0.086	0.030	0.025	0.019
22	1.620	0.922	0.259	0.055	0.028	0.018
45	3.240	2.270	0.449	0.184	0.044	0.023

XRPD patterns (note that all XRPD patterns were measured using $Co_{K\alpha}$ irradiation) of the quartz sand sample and the SITI composites dried at 105 ºC are shown in Fig. 1.

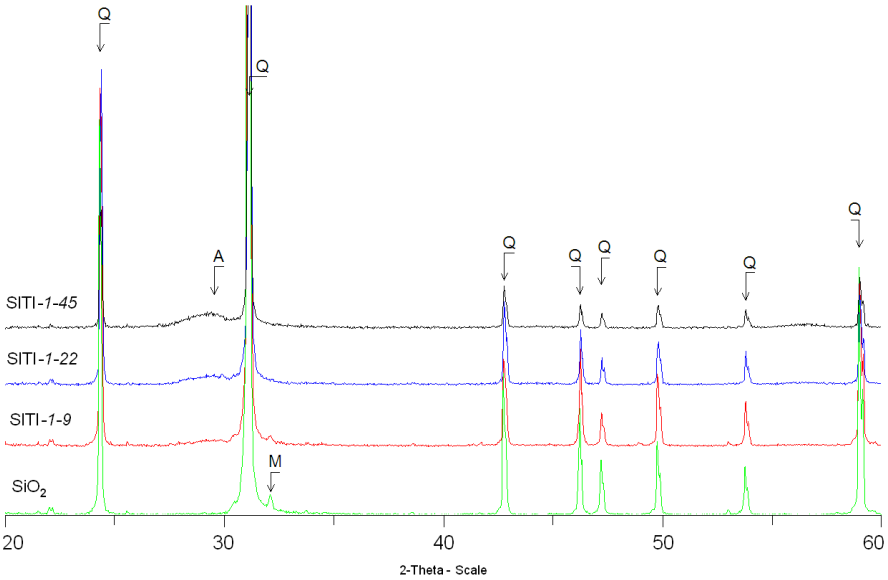

Fig. 1. Comparison of X-ray powder diffractions pattern of pure quartz sand and SITI composites dried at 105°C. Q: SiO_2, M: $KAlSi_3O_8$, A: TiO_2 - anatase form.

Muscovite (M; PDF number 7-0042) represents the typical mineral admixture accompanying pure quartz (Q; PDF number 85-0798). The presence of this admixture is also in agreement with the chemical composition of the original quartz sand sample (see Table 1). In the SITI

composites, the increase of TiO_2–anatase (A; PDF number 86-1157) content led to the decrease of the Q and M fractions and consequently to the decrease of intensity for Q and M peaks. This decrease is the only evidence that SITI-*1-9* contains a TiO_2 because no distinctive TiO_2-anatase peak can be found in this XRPD pattern. For SITI-*1-22* and SITI-*1-45* only one broad, and not very distinctive, TiO_2–anatase peak (101) is evident in the region of 26–29º 2θ (CoK_α) suggesting a low crystallinity of TiO_2 (see Fig. 1).

The XRPD patterns of the SITI samples calcined for 1h at 600ºC are presented in Fig. 2.

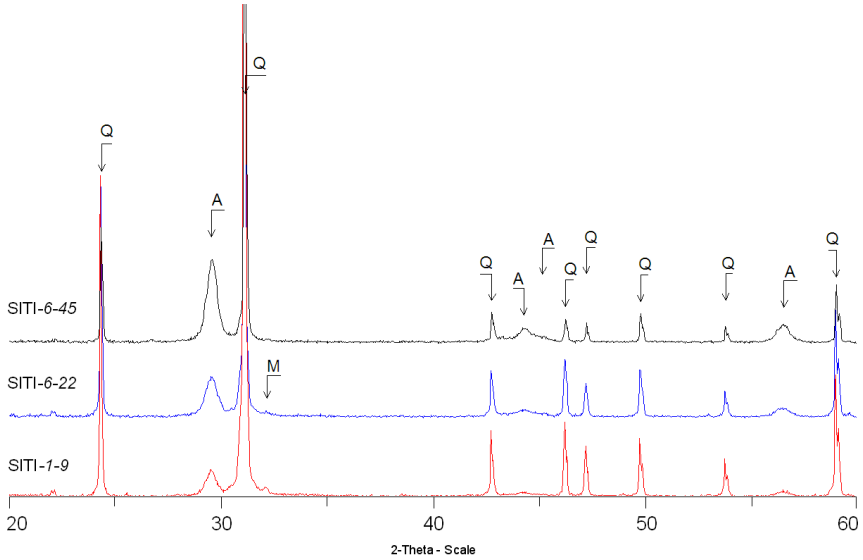

Fig. 2. Comparison of X-ray powder diffraction patterns of SITI composites calcined at 600°C. Q: SiO_2, M: $KAlSi_3O_8$, A: TiO_2 - anatase form.

Comparing the XRPD patterns of composites before and after the calcinations, it is clearly observable that the quartz does not undergo any structure change while the TiO_2-anatase peaks become significant. The presence of the (101) TiO_2-anatase diffraction peak in the region of 26–29º 2θ (CoK_α) is clearly observable for all SITI composites calcined at 600°C. The presence of this peak is caused by the increase of size of the TiO_2 crystallites during the calcination process. The lowering the intensity of M peak (32º 2θ) is caused by the decrease of the fraction of this admixture with the increasing amount of TiO_2.

The XRPD patterns of the SITI samples calcined for 1h at 800ºC are presented in Fig. 3. One can see that quartz still does not undergo any significant changes while TiO_2 starts to transform from the anatase phase into the rutile phase. The comparison of the (101) TiO_2-anatase diffraction peak (26–29º 2θ) in Figs. 2 and 3 reveals the further increase of the anatase crystallites size (see also Table 3). The M peak (32º 2θ) is no longer observable because of the presence of the much more significant (110) TiO_2-rutile diffraction peak.

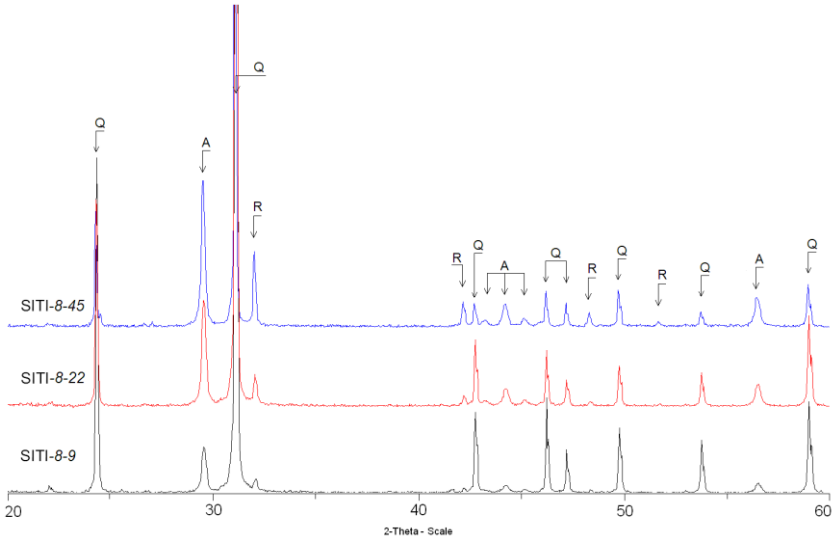

Fig. 3. Comparison of X-ray powder diffraction patterns of SITI composites calcined at 800°C. Q: SiO_2, A: TiO_2 - anatase form, R: TiO_2 - rutile form.

The TiO_2–anatase crystallite size (L_C) for all SITI composites was calculated according to the (101) TiO_2–anatase diffraction peak using the Scherrer formula [28] and the values are shown in Table 3 (lanthanum hexaboride (LaB_6) was used as a standard).

Table 3
The crystallite size L_C [nm] of anatase grows with the temperature of calcination and reaches the maximum for the sample SITI-*9-45*.

TiO_2 content in SITI [wt.%]	temperature [°C]				
	500	600	700	800	900
9	18	25	40	68	101
22	13	21	42	73	105
45	13	20	32	85	160

It is evident that the L_C grows with dependence on the calcination temperature. In the temperature range 500-800 °C the L_C is not significantly affected by an increasing amount of TiO_2 while for SITI-*9-45* the L_C = 160 nm is much higher than for SITI-*9-22* and SITI-*9-9* (L_C ~ 103 nm).

The dependence of the anatase/rutile ratio on the amount of TiO_2 and on the temperature of calcination is clearly shown in Fig. 4. The SITI composites with a lower amount of TiO_2 (i.e. containing 9 and 22 wt.%, respectively) show the appearance of the rutile phase for the first time at 800 ºC, while in the case of the SITI composite containing 45 wt.% of the TiO_2 the rutile phase occurs even at 700 ºC. For all the SITI composites 600 ºC is the highest

calcination temperature at which only the anatase form is present (see Fig. 4). The amount of rutile increases with increasing content of TiO_2 in the SITI composite.

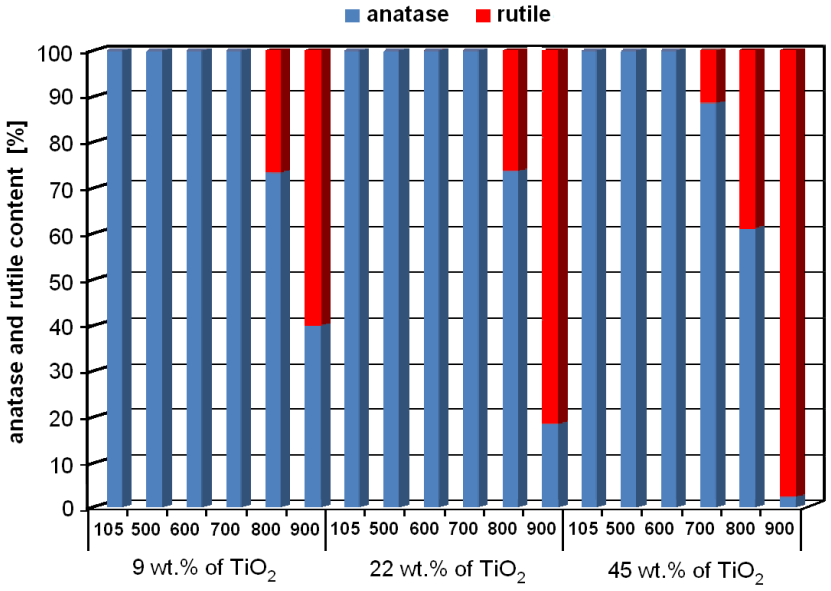

Fig. 4. The anatase and rutile content in all SITI samples depending on drying (105°C) and calcination (500 – 900°C) temperature.

3.2 Infra-red spectra of the prepared composites

Fig. 5 shows the mid-IR spectra of the samples dried at 105 ºC while the mid-IR spectra of the samples calcined at 600 ºC and 800 °C can be found in Fig. 6 and Fig. 7, respectively.

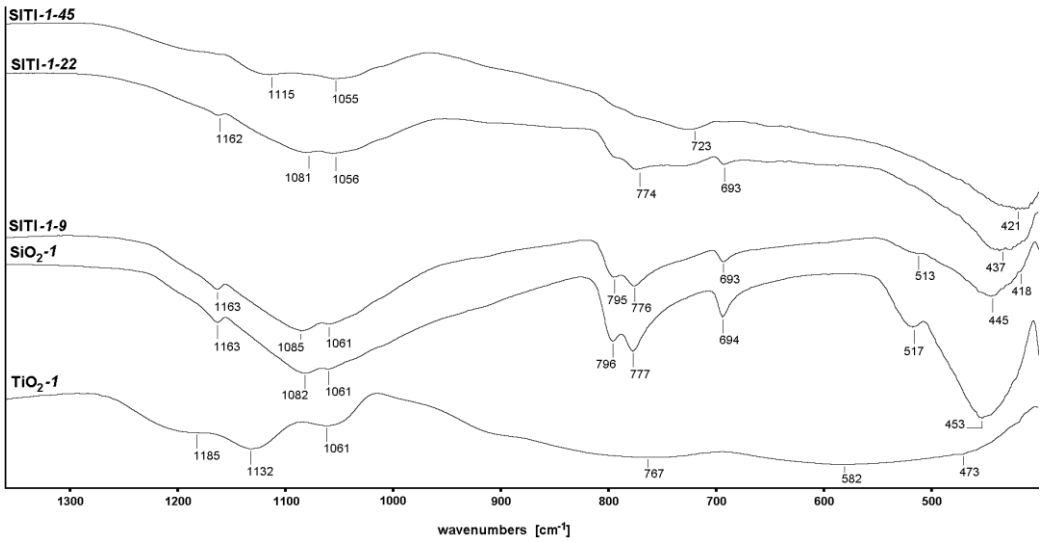

Fig. 5. Mid-IR spectra of the samples dried at 105 °C.

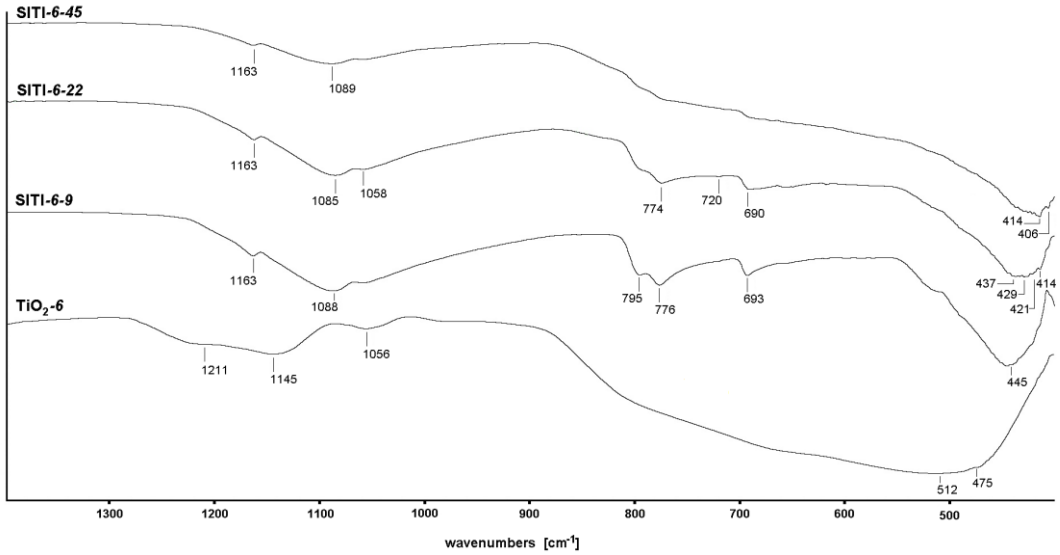

Fig. 6. Mid-IR spectra of the samples calcined for 1h at 600 °C.

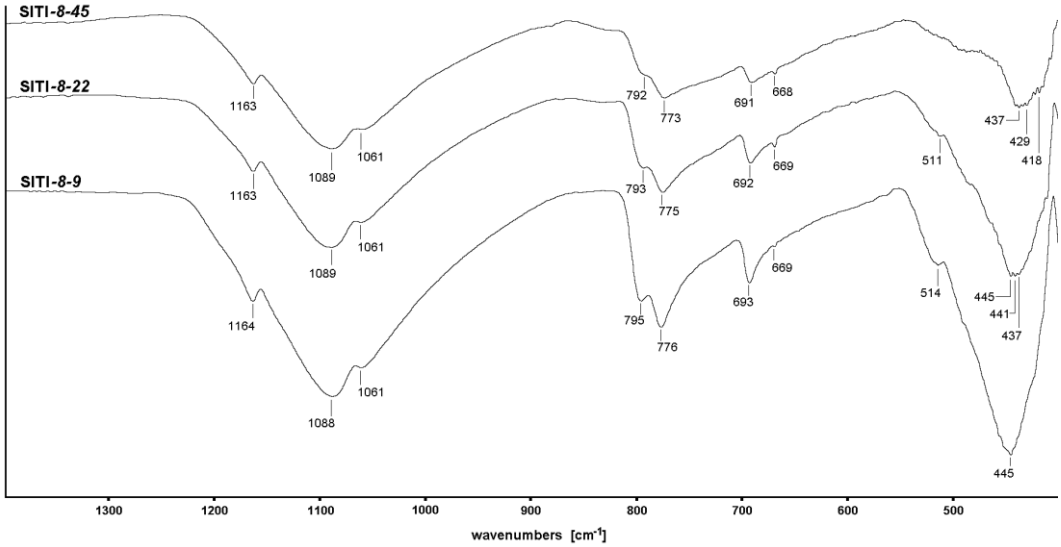

Fig. 7. Mid-IR spectra of the samples calcined for 1h at 800 °C.

The spectra of both dried and calcined TiO_2 have a broad band around 1200 cm^{-1} which may be attributed to vibration of S-O bonds in sulfuric acid remaining in the TiO_2 sample from the used precursor $TiOSO_4$ (see Fig. 5). The spectra of the SITI samples exhibit broad bands at 1160 cm^{-1} corresponding to stretching vibrations in the linear chain of Si-O-Si, and two bands around 1080 cm^{-1}(vibrations of 4-fold and 6-fold SiO_4 rings) and 1050-1060 cm^{-1} (vibrations of 4-fold SiO_4 rings) [29]. The spectra of the pure quartz sand and the samples with lower content of TiO_2 contain a doublet below 800 cm^{-1} characteristic for vibrations of Si-O bonds in quartz.

The characteristic band between 910-960 cm^{-1} attributed to Si–O–Ti antisymmetric stretching vibration [30] was not observed at the recorded spectra of the SITI composites, probably due

to a low abundance of these bonds in the prepared composites. Therefore, computer molecular modeling has been used to at least indirectly confirm the presence of these bonds.

3.3. Composite particles morphology and texture parameters

SEM image of SITI-*6-22* in Fig. 8 reveal that the surface of quartz particles in the SITI composite is fully covered by TiO_2 layer. The cracks caused by the calcination are clearly visible. However, also the aggregates of pure TiO_2 are present. The structure of these aggregates is more obvious in TEM images (see Figs. 9a and 9b).

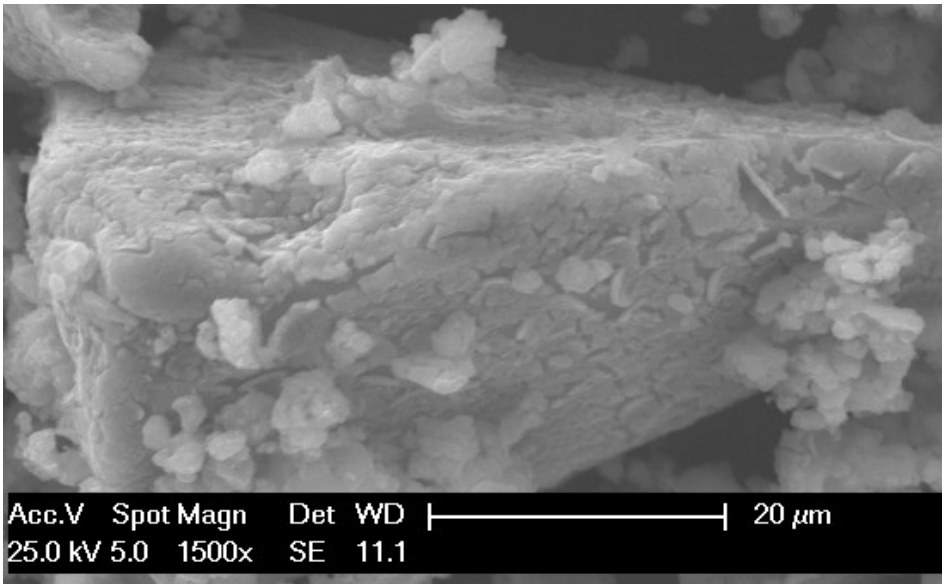

Fig. 8. SEM micrograph of SITI-*6-22* composite.

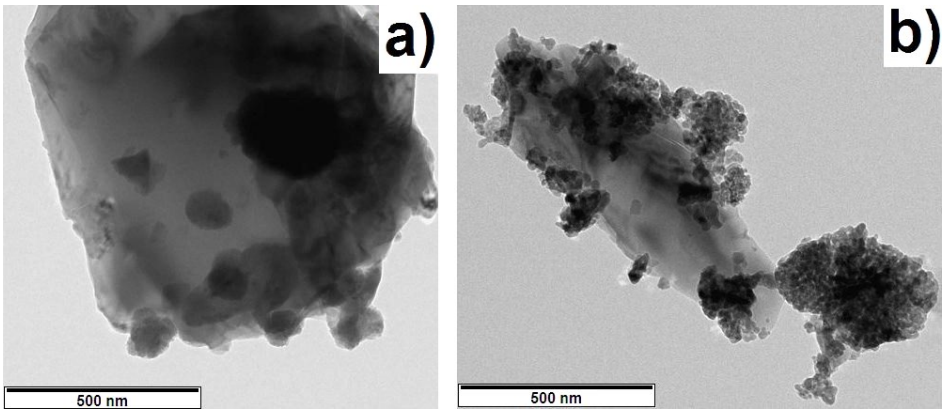

Fig. 9. TEM micrographs of (a) SITI-*1-22* and (b) SITI-*6-22* composites.

The presence of the amorphous TiO_2 clusters in SITI-*1-22* (Fig. 9a) and agglomerates of well-crystallized TiO_2 nanoparticles SITI-*6-22* (Fig. 9b) is in a good agreement with the XRPD patterns in Figs. 1 and 2, respectively. Both Figs. 9a and 9b also reveal that the surface of

quartz in the SITI composite is not fully covered by TiO_2. SSA values for the pure quartz sand (dried and calcined at 600 °C), SITI-*1-X* and SITI-*T-22* composites are shown in Table 4.

Table 4
Comparison of the specific surface area values for the pure quartz sand (SiO_2; dried at 105°C and calcined at 600°C), SITI-*1-X* and SITI-*T-22* composites.

sample	SSA [m^2/g]	sample	SSA [m^2/g]
SiO_2(1)	< 1	SITI-5-22	22.2
SiO_2(6)	< 1	SITI-6-22	18.4
SITI-1-9	10.9	SITI-7-22	11.3
SITI-1-22	38.1	SITI-8-22	9.1
SITI-1-45	105.8	SITI-9-22	4.4

One can see that the SSA values increase with dependence on the TiO_2 amount, which is related to the origination of new TiO_2 surfaces. For the calcined samples the SSA values are significantly lower (for an example, comparing the SSA value for SITI-*1-22* and SITI-*6-22*). The decrease of SSA values with increasing temperature of calcination is in a good agreement with the increasing size of the TiO_2 crystallites (see Tables 3 and 4).

3.4. Determination of photodegradation activity of prepared composites

For the determination of the photodegradation activity the model organic compound AO7 was used. The photodegradation activity of the prepared samples, calculated using Eq. (1), can be seen in Table 5.

Table 5
Photodegradation activities [%] for all dried and calcined SITI samples. Comparison of the photodegradation activity for the SITI-*T-22* composites after 1h and 5h long irradiation with UV light can be seen in the second and third row.

	temperature [°C]					
TiO_2 content in SITI [wt.%]	105	500	600	700	800	900
9	6.5	11.4	5.1	10.3	13.8	-
22 (1h)	7.7	20.2	23.0	26.5	27.6	9.3
22 (5h)	20.0	73.0	70.0	76.0	84.0	31.0
45	9.1	22.7	21.8	25.6	19.4	-

At first the photodegradation activity of the SITI-*T-X* composites has been evaluated after the 1h long UV irradiation. Comparing the results obtained it is evident that the SITI-*T-9*

composites shows the lowest photodegradation activities, which ranges from 6.5 – 13.8 %. The maximum photodegradation activity after 1 h long irradiation 27.6 % was observed for the SITI-*8-22* composite (the composite with 19 wt.% of TiO_2 calcined at 800 °C). Significantly higher content of TiO_2 in SITI-*T-45* composite (40 wt.% of TiO_2) did not enhance the photodegradation activity as evident from Table 5, slightly higher photodegradation activity shows only the SITI-*1-45* and SITI-*5-45* composites. Taking into account the results of photodegradation activity obtained after 1h long irradiation, the composites with 19 wt.% of TiO_2 were selected for photodegradation tests using 5h long UV irradiation. Comparing the extent of AO7 photodegradation after 1 and 5 h long irradiation tested for composites SITI-*T-22* it is evident, that the prolonged irradiation has significant effect on degradation of AO7 and that the highest extent of photodegradation of AO7 shows the composite SITI-*8-22*. Kamaruddin and Stephan [31] studied the photodegradation activity of quartz-TiO_2 composites (containing 10, 20, 30 and 40 wt.% of TiO_2) prepared using titanium tetrapropylate as TiO_2 precursor. They used methylene blue (MB) as the model organic compound and observed the highest photodegradation activity for the composite calcined at 650 °C and containing 20 wt.% of TiO_2 which showed approx. 85% decrease in initial MB concentration after 10h long irradiation. Although it is not possible to directly compare the photodegradation activity of the SITI composites with the composites prepared by Kamaruddin and Stephan (the setup of photodegradation testing is different) both studies shows the quartz-TiO_2 composites as photocatalytically active and similarly indicate the composites with approx. 20 wt.% of TiO_2 calcined at the temperatures higher than 600 °C as the best performing.

Analyzing the data obtained during the characterization of the prepared SITI composites it is difficult to find the explanation why the SITI-*8-22* composite is the best performing one. Taking into account all of the data it can be outlined the possible synergic effect of amount of the mixed anatase-rutile structure when SITI-*8-22* consists of approx. 72 % of anatase and 28 % of rutile which makes this composite the best performing one. Similar observation reported e.g. Bakardjieva et al. [32], where the authors reported the highest photodegradation activity against 4-chlorphenol for the TiO_2 sample consisting of anatase/rutile (77%/23%) mixed structure which was achieved after the calcination of the pure anatase at 825°C. The calcination of the SITI composite at the temperature 900°C promote the anatase-rutile transformation what has a detrimental effect on the photodegradation activity of the composite SITI-*9-22* as is evident from Table 5.

3.5. Study of the structure and adhesion forces using molecular modeling

The molecular modeling with an empirical force field as implemented in MS was used to confirm the presence of Ti-O-Si bonds in SITI composites. Despite the fact that no new chemical bonds can form in systems treated by molecular mechanics, they are easily inferred to exist based on the distances between atoms [33]. Therefore, in addition to computing the adhesion energies, special attention has been paid to the measurement of distances between Ti atoms from the base of TiO_2 nanoparticles and O atoms from adjacent SiO_2 surface.

Three SiO_2 substrates (quartz alpha [34]) were built as non-periodic superstructures (see Fig. 10) by cleaving the structure along (001), (011) and (111) crystallographic planes. The formula of each substrate was Si_{3442} O_{6888} with the total charge x = -8 el.

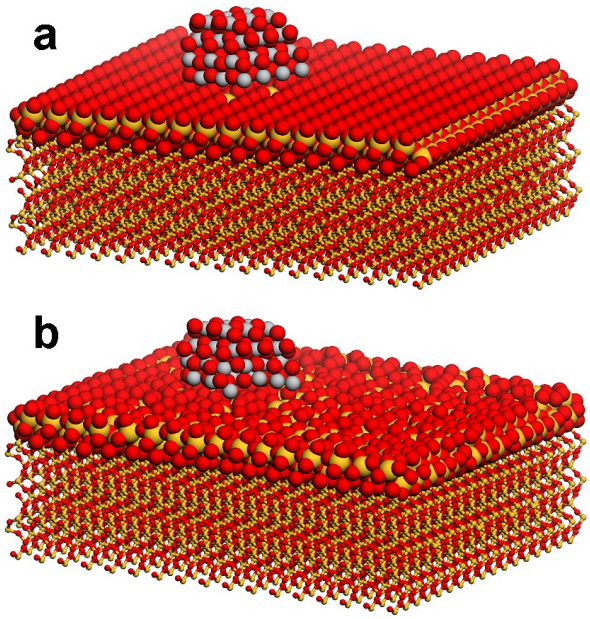

Fig. 10. (a) Initial $SiO_2(001)/TiO_2(001)$ model. Imperfect crystal structure of the $SiO_2(001)$ surface can be seen under the $TiO_2(001)$ nanoparticle; (b) optimized $SiO_2(001)/TiO_2(001)$ model. Fixed and unfixed atoms are displayed in balls-and-stick and van der Waals diameter mode, respectively. Colors: O – red; Si – beige; Ti – grey.

This charge comes from the lack of atoms (4 silicon atoms and 4 oxygen atoms are missing). These atoms are removed from the SiO_2 surface in order to obtain the site with imperfect crystal structure (see Fig. 10a). The site with a lack of atoms may originate on the SiO_2 surface due to chemical attack by sulfuric acid, which is the main component of the $TiOSO_4$ colloid suspension [35].

The SiO_2 substrate models are denoted as $SiO_2(001)$, $SiO_2(011)$ and $SiO_2(111)$. The average size of each SiO_2 substrate is 9.0 nm × 9.0 nm. The thickness of each SiO_2 substrate is 2 nm. In each SiO_2 substrate the bottom atomic layers (7737 atoms) representing bulk material are

fixed. Thicknesses of non-fixed top atomic layers are 0.5 nm (2593 atoms) for each SiO_2 substrate.

Three types of TiO_2 nanoparticles (anatase structure [36]) were prepared with various crystallographical orientations against the SiO_2 substrates. These orientations were (001), (100) and (110). Each TiO_2 nanoparticle has 113 atoms ($Ti_{39}O_{74}$) a and total charge of x = +8 el. For more details about the prepared TiO_2 nanoparticles, see Table 6.

Table 6
Characteristics of nanoparticles prepared for the initial TiO_2/SiO_2 models. Value d is the size of nanoparticles in the diagonal direction of the basal planes; h is the height of the nanoparticle; n is the number of atoms in nanoparticle.

nanoparticles	n	d [nm]	h [nm]
TiO_2(001)	133	1.7	1.1
TiO_2(100)	133	1.7	1.0
TiO_2(110)	133	2.0	0.6

The similarity of the nanoparticles with different crystallographic orientations for possible comparison was warranted by the fulfillment of the two following conditions: (a) the same number of atoms in whole nanoparticle and (b) the same number of atoms in the plane adjacent to the SiO_2 substrate (12 titanium and 12 oxygen atoms). Because the distribution of atoms in various crystallographic planes is not the same, the second condition constrained each nanoparticle to have a different size in the diagonal direction of the basal planes (see Table 6).

Initial models of the SITI composite were prepared by anchoring each TiO_2 nanoparticle onto two sites (either imperfect or perfect crystal structure) of each SiO_2 substrate. The surfaces of SiO_2 are large enough to keep the TiO_2 nanoparticle anchored on the site with perfect structure unaffected by the site with imperfect crystal structure and by the substrate margin (see Fig. 10). Thus it is possible to compare the adhesion forces for TiO_2 nanoparticles anchored on both types of sites.

QEq (charge equilibration) method in *MS* was used to calculate the atomic charges [37]. The interaction between nanoparticles and substrate is quantified using the adhesion energy

$$E_{ad} = (E_{tot,TiO2} + E_{tot,SiO2}) - E_{tot} \quad (2)$$

where E_{tot} is the total energy of the composite (i.e., the TiO_2 nanoparticle anchored on the SiO_2 substrate). $E_{tot,TiO2}$ is the total energy of the TiO_2 nanoparticle and $E_{tot,SiO2}$ is the total energy of the SiO_2 substrate. These energies are expressed in the unit [kJ] and have been

calculated using the UFF [38] in the *MS Forcite* module. In our previous works the UFF proved to be the suitable force field for the modeling of such type (i.e. silicate/nanoparticle) of composites [33,39,40].

The models have been optimized using UFF in the *MS Forcite* module. A smart algorithm (i.e. the cascade of Steepest descent, Conjugate gradient and Quasi-Newton optimization algorithms) was used for the geometry optimization with 50,000 iteration cycles.

Nine initial models have been prepared, optimized and examined. This number does not include modifications via shifting and rotations of the TiO_2 nanoparticles along the substrate in order to obtain better optimization results. In fact, more than fifty models were studied.

The optimized models revealed that in both cases (i.e. TiO_2 nanoparticles anchored on perfect or imperfect SiO_2 sites) TiO_2(001) nanoparticle exhibits the strongest adhesion while TiO_2(110) nanoparticle exhibits weak adhesion. The highest and the lowest adhesion energies computed using Eq. (2) are in good agreement with the values of average distances between Ti atoms from the base of TiO_2 nanoparticles and O atoms from SiO_2 surfaces. The higher adhesion energies, the shorter average distance (see Table 7).

Table 7
Adhesion energies calculated from models containing TiO_2 nanoparticles anchored on either the perfect site of SiO_2 substrate without surface defect or the imperfect site of SiO_2 substrate without surface defect. Average distances between Ti atoms from the base of TiO_2 nanoparticle and O atoms from SiO_2 surface ($d_{Ti...O}$) together with the shortest measured $d_{Ti...O}$ distances are also listed.

models	adhesion energy [kJ·mol^{-1}]		average $d_{Ti...O}$ (shortest $d_{Ti...O}$) [nm]	
	perfect site	imperfect site	perfect site	imperfect site
TiO_2(001) / SiO_2(001)	36282	36211	0.249 (0.232)	0.243 (0,191)
TiO_2(100) / SiO_2(001)	34861	35655	0.282 (0,241)	0.261 (0,205)
TiO_2(100) / SiO_2(011)	29498	30481	0.351 (0,332)	0.294 (0,225)
TiO_2(110) / SiO_2(001)	23724	30281	0.359 (0,329)	0.324 (0.299)

One can see the stronger adhesion forces between TiO_2 nanoparticles and SiO_2 imperfect sites with one exception - TiO_2(001)/SiO_2(001) model - in the first row, where the adhesion energies are nearly the same in both cases of perfect and imperfect sites of SiO_2(001) substrate. Nevertheless, the average distance is shorter for the imperfect site. The optimized TiO_2(001)/SiO_2(001) model can be seen in Fig. 10b.

Average distances in Table 7 are presented together with values of the shortes distances measured in the models. Taking into account that the lengths of Ti-O and Si-O bonds are 0.1973 (or 0.1930) and 0.1522 nm [34,36], respectively, the formation of Ti-O-Si bonds can

be assumed in the $TiO_2(001)$ / $SiO_2(001)$ model and very probably also in the $TiO_2(100)$ / $SiO_2(001)$ model. Therefore, computer molecular modeling at least indirectly proved the presence of Ti-O-Si bonds and revealed the most probable mutual crystallographic orientations of TiO_2 and SiO_2 adjacent surfaces.

4. Conclusions

In the preparation process of the photoactive SITI composites, we used $TiOSO_4$, the widely accessible intermediate from the sulfate process of TiO_2 pigment manufacturing, as a cheap precursor of TiO_2. In order to minimize the environmental risks of TiO_2 nanoparticles and to make the manipulation of this material easier and safer, the TiO_2 nanoparticles were anchored to larger particles of pure quartz sand. It was proved that the anchoring does not affect the photoactivity of TiO_2 nanoparticles. Such prepared SITI composite represents a promising material, which is suitable for use in wide range of building materials containing both TiO_2 and sand (i.e. plasters, etc.). The future plan of our research group is to prepare the mortars based on white cement enriched with TiO_2.

Obtained results can be briefly summarized as follows.

1) The quartz sand/TiO_2 composites were successfully prepared using the low cost precursor $TiOSO_4$, whereas the yield reaches approx. 87 % with respect to the assumed content of TiO_2. It was observed that the content of the sulfur grows with an increase of TiO_2 content, and decreases with the temperature of heat treatment. Minimal temperature for anatase to rutile transformation occurs at 700 °C in the composite with 39 wt.% of TiO_2. Anatase crystallite size increases with calcination temperature and reaches 160 nm in the case of the composite with SITI-*9-45* (composite with 39 wt.% of TiO_2 calcined at 900 °C).
2) Calcination at 800°C caused an increase in the photodegradation activity of the SITI composite containing 22 wt.% of TiO_2. This SITI-*8-22* composite contains about 28 wt.% of rutile in the total volume of TiO_2, which is similar to the standard Degussa P-25 powder containing 25 wt.% of rutile. The longer irradiation time led to the significant increase (more than 100%) of the photodegradation activity.
3) The photodegradation activity of the SITI samples decreases rapidly when more than 50 wt.% of rutile is present in the total volume of TiO_2 in sample and also when the size of TiO_2 nanoparticles becomes larger than 100 nm.
4) The fact, that SITI-*T-22* composites (calcined at 600°C, 700°C or 800°C) exhibits higher photodegradation activity than SITI-*T-45* composites calcined at the same

temperatures is the result which is in very good agreement with our intention to find the photoactive TiO_2/SiO_2 composite with optimum price-efficiency ratio.

5) The presence of Si-O-Ti bond was not observed at the recorded IR spectra, probably due to a small number of these bonds in prepared SITI composites. However, the presence of Si-O-Ti bonds has been proved indirectly by computer molecular modeling.

Acknowledgement

This work was supported by the European Regional Development Fund in the IT4Innovations Centre of Excellence project (CZ.1.05/1.1.00/02.0070) and Ministry of Education of Czech Republic (SP2012/47 and SP2013/67). This paper has been also elaborated in the framework of the "Regional Materials Science and Technology Centre" project reg. No. CZ.1.05/2.1.00/01.0040 supported by Operational Programme "Research and Development for Innovations" and in the framework of the Nanotechnology – the basis for international cooperation project, reg. No. CZ.1.07/2.3.00/20.0074 supported by Operational Programme 'Education for competitiveness' and financed by the Structural Funds and from the state budget of the Czech Republic.

References

[1] U. Diebold, The surface science of titanium dioxide, Surf. Sci. Rep. 48 (2003) 53-229.

[2] A. Fujishima, X. Zhang, D.A. Tryk, TiO_2 photocatalysis and related surface phenomena, Surf. Sci. Rep. 63 (2008) 515-582.

[3] C. Xiabo, S.S. Mao, Synthesis of titanium dioxide (TiO_2) nanomaterials, J. Nanosci. Nanotechnol. 6 (2006) 906–925.

[4] M. Asiltürk, F. Sayılkan, S. Erdemoğlu, M. Akarsu, H. Sayılkan, M. Erdemoğlu, E. Arpac, Characterization of the hydrothermally synthesized nano-TiO_2 crystallite and the photocatalytic degradation of rhodamine B, J. Hazard. Mater. 129 (2006) 164-170.

[5] J. Klongdee, W. Petchkroh, K. Phuempoonsathaporn, P. Praserthdam, A.S. Vangnai, V. Pavarajarn, Activity of nanosized titania synthesized from thermal decomposition of titanium (IV) n-butoxide for the photocatalytic degradation of diuron, Sci. Technol. Adv. Mater. 6 (2005) 290-295.

[6] M. Bellardita, M. Addamo, A. Di Paola, G. Marci, L. Palmisano, L. Cassar, M. Borsa, Photocatalytic activity of TiO_2/SiO_2 systems, J. Hazard. Mater. 174 (2010) 707-713.

[7] J. Zou, J. Gao, H_2O_2-sensitized TiO_2/SiO_2 composites with high photocatalytic activity under visible irradiation, J. Hazard. Mater. 185 (2011) 710–716.

[8] D.V. Bavykin, V.P. Dubovitskaza, A.V. Vorontsov, V.N. Parmon, Effect of $TiOSO_4$ hydrothermal hydrolysis conditions on TiO_2 morphology and gas-phase oxidative activity, Res. Chem. Intermed. 33 (2007) 449-464.

[9] T. Ginsberg, M. Modigell, W. Wilsmann, Thermochemical characterisation of the calcination process step in the sulphate method for production of titanium dioxide, Chem. Eng. Res. Des. 89 (2011) 990-994.

[10] M.V. Phanikrishna Sharma, G. Sadanandam, A. Ratnamala, V.D. Kumari, M. Subrahmanyam, An efficient and novel porous nanosilica supported TiO_2 photocatalyst for pesticide degradation using solar light, J. Hazard. Mater. 171 (2009) 626–633.

[11] N. Kashif, F. Ouyang, Parameters effect on heterogeneous photocatalysed degradation of phenol in aqueous dispersion of TiO_2, J. Environ. Sci. 21 (2009) 527-533.

[12] Q. Yhang, L. Gao, Preparation of nanocrystalline TiO_2 powders for photocatalytic oxidation of phenol, Res. Chem. Intermed. 35 (2009) 281-286.

[13] F. Han, V.S. Rao Kambala, M. Srinivasan, D. Rajarathnam, R. Naidu, Tailored titanium dioxide photocatalysts for the degradation of organic dyes in wastewater treatment, Appl. Catal., A 359 (2009) 25-40.

[14] A. Hilonga, J.K. Kim, P.B. Sarawade, H.T. Kim, Rapid synthesis of homogeneous titania-silica composite with high-BET surface area, Powder Technol. 199 (2010) 284-288.

[15] K. Dai, H. Chen, T. Peng, D. Ke, H. Yi, Photocatalytic degradation of methyl orange in aqueous suspension of mesoporous titania nanoparticles, Chemosphere 69 (2007) 1361-1367.

[16] T.X. Liu, F.B. Li, X.Z. Li, TiO_2 hydrosols with high activity for photocatalytic degradation of formaldehyde in a gaseous phase, J. Hazard. Mater. 152 (2008) 347–355.

[17] G. Colón, M. Maicu, M.C. Hidalgo, J.A. Navío, A. Kubacka, M. Fernández-García, Gas phase photocatalytic oxidation of toluene using highly active Pt doped TiO_2, J. Mol. Catal. A: Chem. 320 (2010) 14-18.

[18] R.B. Zhang, Photodegradation of toluene using silica-embedded titania, J. Non-Cryst. Solids 351 (2005) 2129-2132.

[19] Z. Wu, H. Wang, Y. Liu, Z. Gu, Photocatalytic oxidation of nitric oxide with immobilized titanium dioxide films synthesized by hydrothermal method, J. Hazard. Mater. 151 (2008) 17–25.

[20] M. Heinlaan, A. Ivask, I. Blinova, H.-C. Dubourguier, A. Kahru, Toxicity of nanosized and bulk ZnO, CuO and TiO_2 to bacteria *Vibrio fischeri* and crustaceans *Daphnia magna* and *Thamnocephalus platyurus*, Chemosphere 71 (2008) 1308-1316.

[21] D. Xiong, T. Fang, L. Yu, X. Sima, W. Zhu, Effects of nano-scale TiO_2, ZnO and their bulk counterparts on zebrafish: Acute toxicity, oxidative stress and oxidative damage, Sci. Total Environ. 409 (2011) 1444-1452.

[22] X. Zhu, Y. Chang, Y. Chen, Toxicity and bioaccumulation of TiO_2 nanoparticle aggregates in Daphnia magna, Chemosphere 78 (2010) 209-215.

[23] T.V. Nguyen, H.C. Lee, M. Alam Khan, O.B. Yang, Electrodeposition of TiO_2-SiO_2 nanocomposite for dye-sensitized solar cell, Solar Energy 81 (2007) 529-534.

[24] S. Mu, Y. Long, S.Z. Kang, J. Mu, Surface modification of TiO_2 nanoparticles with a C60 derivative and enhanced photocatalytic activity for the reduction of aqueous Cr(VI) ions, Catal. Commun. 11 (2010) 741-744.

[25] A. Kafizas, S. Kellici, J.A. Darr, I.P. Parkin, Titanium dioxide and composite metal/metal oxide titania thin films on glass: a comparative study of photocatalytic activity, J. Photochem. Photobiol. A 204 (2009) 183-190.

[26] T. Watanabe, A. Nakajima, R. Wang, M. Minabe, S. Koizumi, A. Fujishima, K. Hashimoto, Photocatalytic activity and photoinduced hydrophilicity of titanium dioxide coated glass, Thin Solid Films 351 (1999) 260-263.

[27] S. Zhu, D. Zhang, X. Zhang, L. Zhang, X. Ma, Y. Zhang, M. Cai, Sonochemical incorporation of nanosized TiO_2 inside mesoporous silica with high photocatalytic performance, Microporous Mesoporous Mater. 126 (2009) 20-25.

[28] P. Scherrer, Estimation of size and internal structure of colloidal particles by means of Rontgen rays, Nachr. Ges. Wiss. Gottingen (1918).

[29] I.P. Lisovsky, V.G. Litovchenko, D.O. Mazunov, S. Kaschieva, J. Koprinarova, S.N. Dmitriev, Infrared spectroscopy study of Si-SiO_2 structures irradiated with high-energy electrons, J. Opt. Adv. Mat. 7 (2005) 325-328.

[30] X. Gao, I.E. Wachs, Titania – silica as catalysts: molecular structural characteristics and physico-chemical properties, Catal. Today 51 (1999) 233-254.

[31] S. Kamaruddin, D. Stephan, Quartz–titania composites for the photocatalytical modification of construction materials, Cement Concrete Comp. (2012), http://dx.doi.org/10.1016/j.cemconcomp.2012.08.007.

[32] S. Bakardjieva, J. Šubrt, V. Štengl, M.J. Dianez, M.J. Sayagues, Photoactivity of anatase–rutile TiO_2 nanocrystalline mixtures obtained by heat treatment of homogeneously precipitated anatase, Appl. Catal., B 58 (2005) 193-202.

[33] J. Tokarský, P. Čapková, J.V. Burda, Structure and stability of kaolinite/TiO_2 nanocomposite: DFT and MM computations, J. Mol. Model. 18 (2012) 2689-2698.

[34] J.D.H. Donnay, Y. Le Page, The vissisitudes of the low-quartz crystal setting or the pitfalls of enantiomorphisms. Acta Crystallogr., Sect. A 34 (1978) 584-594.

[35] A.K. Panda, B.G. Mishra, D.K. Mishra, R.K. Singh, Effect of sulphuric acid treatment on the physicochemical characteristics of kaolin clay. Colloids Surf., A 363 (2010) 98-104.

[36] C.J. Howard, T.M. Sabine, F. Dickson, Structural and thermal parameters for rutile and anatase. Acta Crystallogr., Sect. B 47 (1991) 462-468.

[37] A.K. Rappe, W.A. Goddard, Charge equilibration for molecular dynamics simulations, J. Phys. Chem. 95 (1991) 3358-3363.

[38] A.K. Rappe, C.J. Casewit, K.S. Colwell, W.A. Goddard, W.M. Skiff, UFF, a full periodic table force field for molecular mechanics and molecular dynamics simulations, J. Am. Chem. Soc. 114 (1992) 10024-10035.

[39] K. Mamulová Kutláková, J. Tokarský, P. Kovář, S. Vojtěšková, A. Kovářová, B. Smetana, J. Kukutschová, P. Čapková, V. Matějka, Preparation and characterization of photoactive composite kaolinite/TiO_2, J. Hazard. Mater. 188 (2011) 212-220.

[40] V. Matějka, M. Šupová, V. Klemm, D. Rafaja, M. Valášková, J. Tokarský , J. Lešková, E. Plevová, Vermiculite interlayer as a reactor for CdS ultrafine particles preparation, Microporous Mesoporous Mater. 129 (2010) 118-125.